Atmos. Meas. Tech. Discuss., 8, 487–516, 2015
www.atmos-meas-tech-discuss.net/8/487/2015/
doi:10.5194/amtd-8-487-2015

Atmospheric Measurement Techniques Discussions
Open Access

Comparing OMI UV index to ground-based measurements at two Finnish sites with focus on cloud-free and overcast conditions

M. R. A. Pitkänen[1], A. Arola[1], K. Lakkala[2], T. Koskela[3], and A. V. Lindfors[1]

[1]Finnish Meteorological Institute, P.O. Box 1627, 70211, Kuopio, Finland
[2]Finnish Meteorological Institute, Tähteläntie 62, 99600, Sodankylä, Finland
[3]Finnish Meteorological Institute, P.O. Box 503, 00101, Helsinki, Finland

Received: 28 October 2014 – Accepted: 14 December 2014 – Published: 14 January 2015

Correspondence to: M. R. A. Pitkänen (mikko.pitkanen@fmi.fi)

Published by Copernicus Publications on behalf of the European Geosciences Union.

Abstract

Satellite based surface UV product of the Ozone Monitoring Instrument OMI was validated using ground based UV measurements from the two Finnish sites Jokioinen and Sodankylä. The goal was to further investigate the observed positive UV bias of the OMI UV product focusing on how it may be connected to cloudiness during the overpass of the Aura satellite. A total of seven years of summer time data was used to compare OMI UV index to a reference UVI observed on the ground with Solar Light 501 broadband radiometers. Cloudiness during satellite overpass was determined with auxiliary ground based observations on sunshine duration, cloud cover and global radiation as well as the satellite based MODIS cloud cover estimates. The analysis aimed to minimize the error sources from temporal discrepancies and from the differences in the field of view of OMI and its ground based reference data. As a result, OMI UV product was seen to overestimate surface UV index by 21 % in average and overcast UV index up to 56 %. The study confirms that OMI UV index is overestimated compared to ground based reference, and shows, that the bias is related to cloudiness and is higher during well defined overcast conditions.

1 Introduction

Ozone Monitoring Instrument OMI has been measuring scattered shortwave solar radiation onboard the polar orbiting NASA EOS Aura satellite since 2004 and has produced, among other things, global estimates on UV radiation reaching the earth surface. OMI continues the long UV and ozone time series of its predecessors TOMS instruments since 1978 (Ialongo et al., 2011).

Tanskanen et al. (2006) presents the principle of OMI UV algorithm. First, the clear sky surface UV irradiance is modelled and then corrected for attenuation by clouds, which is estimated by combining information from a radiation transfer model and OMI radiance measurements. The resulting cloud attenuated surface UV irradiance data

AMTD
8, 487–516, 2015

contributes to long UV time series of TOMS instruments and can help quantifying the long term changes in UV radiation on a global scale (Ialongo et al., 2011).

Since Aura was launched in 2004, efforts have been made to estimate possible uncertainties in the operational UV data and enhance the quality of the product. While the UV product is generally of good quality, it has been shown to overestimate surface UV compared to ground based instruments in snow free conditions. Kazadzis et al. (2009b), Cachorro et al. (2010) and Ialongo et al. (2008) found OMI erythemal UV dose rate to be overestimated in cloud free cases by about 20 % and less and the highest overestimation can in urban clear sky conditions be partly explained by aerosol absorption.

When cloudy cases are included, however, the overestimation by OMI has proven to be larger, typically over 30 % and up to more than 50 % (Anton et al., 2010; Buchard et al., 2008; Weihs et al., 2008; Kazadzis et al., 2009a; Ialongo et al., 2008) which suggests that clouds are somehow related to increased positive bias in OMI UV products. However, more detailed analysis is needed to explain how clouds may cause the bias considering the radiative transfer conditions. For instance, comparing surface observations to OMI UV index should be done at the time of the satellite overpass, otherwise an additional challenge of changing cloud field between noon and satellite overpass will occur (Ialongo et al., 2008). Also, simplified classification of cloudiness (clear sky vs. all sky situations) (Anton et al., 2010; Ialongo et al., 2008; Kazadzis et al., 2009b) do not allow to infer what type of cloudiness the UV bias might relate to. The relation of the UV bias to spatial variability of cloudiness within an OMI footprint was further investigated by Kazadzis et al. (2009b) and Weihs et al. (2008), but fully overcast situations were presented in their data sets in limited numbers. On the other hand, broken cloudiness makes the OMI to ground based comparison difficult due to high variation of the UV intensity reaching the surface (Kazadzis et al., 2009b). Overall, earlier studies have related cloudiness to a larger positive UV bias in the OMI UV product, but few clues exist on how and in what spesific cloud conditions the bias occurs. For example,

AMTD
8, 487–516, 2015

it is yet to be shown, whether this positive UV bias in overcast situations is due to clear sky areas within an OMI footprint, but unnoticed by ground based instruments.

This work is an attempt based on observations to further investigate the positive UV index bias in OMI UV product. We focused on how the UV index bias is related to cloudiness, that was described by several instruments at once. The specific focus was on clear sky and overcast conditions to simplify the problem so, that both instrument would have entirely cloud free or entirely cloud covered view.

We utilized a seven year dataset of OMI satellite UV product and ground based UV index measurements at two Finnish sites, Jokioinen and Sodankylä. To have a reliable and comparable ground based reference UV index, we used time averages of radiometer data near the satellite overpass, which is an attempt to account for both the rapid variations in cloudiness as well as the spatial discrepancy of the satellite and ground based field of view. Ancillary ground based measurements of sunshine duration, cloudiness and global radiation were used to systematically separate different cloudiness situations (clear sky, broken sky, overcast) in a comprehensive way. This cloudiness classification was supported with MODIS satellite cloud fraction product for an additional high resolution view over an area resembling the OMI satellite footprint.

The data and the methods of UV comparison and cloudiness classification are described in Sect. 2. Section 3 shows the results of our efforts to scrutinize the cloud related OMI bias, which is finally concluded in Sect. 4.

2 Data and methods

This section describes the OMI satellite UV index data and its computational algorithm as well as the method and data of the UV comparison. The ground based reference UV index was obtained with Solar light 501 radiometers, which were calibrated using simultaneous measurements from Brewer spectrophotometers. To classify the cloudiness during satellite overpasses, we used sunshine duration, synoptic cloudiness observation (from ceilometer and visual observation) and variation of global radiation

AMTD
8, 487–516, 2015

(pyranometer) and, further, this classification was supported by MODIS cloud fraction product. Both stations, Jokioinen and Sodankylä, provided the measurements from all corresponding instruments during summers 2005 to 2011.

2.1 OMI satellite UV data

The satellite OMI UV data was selected for two Finnish ground based UV measurement stations Jokioinen (60.8° N, 23.5° E) and Sodankylä (67.3° N, 26.6° E) for the years 2005 to 2011. Only data from snow free seasons (May–September in Jokioinen, June–September in Sodankylä) was included to avoid problems in OMI cloud correction related to bright snow cover (Krotkov et al., 2001).

From OMUVB product we obtained the cloud corrected UV index UVI_{OMI}. This data is available in Aura Validation Data Center (http://avdc.gsfc.nasa.gov/) for many ground stations including Jokioinen and Sodankylä.

Additionally, clear sky UVI at overpass time $UVI_{OMI,cs}$ was used to calculate cloud modification factor CMF = $UVI_{OMI}/UVI_{OMI,cs}$ and thus, to have information on cloud attenuation in the OMI product. $UVI_{OMI,cs}$ was obtained from the operational UV algorithm with nominal modifications and by using the L2 OMTO3 ozone data as model input. The operational L2 OMTO3 data and the corresponding UV data L2 OMUVB are available from Mirador database (http://mirador.gsfc.nasa.gov/).

Tanskanen et al. (2006) describe the OMI UV algorithm in short and a detailed manual is provided in Stammes and Noordhoek (2002). The algorithm estimates for surface UV irradiances are defined from look-up tables representing radiative transfer calculations for surface UV radiation, OMI viewing geometry and cloud attenuation. First, the theoretical cloud free surface irradiance is modelled and it depends essentially on solar zenith angle, surface albedo from climatology and ozone from the OMI ozone product L2 OMTO3. Second, cloud optical thickness τ_c at 360 nm is determined by simulating OMI radiances for different τ_c and then fitting the simulated radiance to the one measured by OMI. The radiances are simulated for a wide range of conditions spanning over the probable ranges of ozone column, surface albedo, viewing geometry, satellite

AMTD
8, 487–516, 2015

measured radiance and τ_c. Third, UV attenuation by clouds is calculated as CMF for the corresponding τ_c, and CMF is lastly multiplied by the cloud free surface irradiance to obtain the attenuated surface irradiance. The result is UVI_{OMI}, that is the validated quantity in this study.

When determining τ_c and cloud attenuation, OMI algorithm assumes a homogeneous plane parallel cloud (PPA) consisting of liquid cloud droplets between 3.5–5 km Krotkov et al. (2001), which was changed from the previous TOMS algorithms that assumed clouds as lambertian reflectors (LER). The clouds in OMI algorithm are embedded in a scattering molecular atmosphere with ozone absorption and, while τ_c is considered a spectrally invariant property of the cloud layer, CMF is wavelength dependent due molecular scattering and ozone absorption (see for example Lindfors and Arola, 2008).

It has been suggested, that the absorption of UV radiation by aerosols may be a large source of uncertainty in satellite UV products in polluted environments (for example Arola et al., 2005; Cachorro et al., 2010). Two different approaches for correcting absorbing aerosols have been applied to OMI UV products so far: the previous aerosol index based correction (Tanskanen et al., 2006) and the currently available climatological correction (Arola et al., 2009). However, according to Aaltonen et al. (2012) the average aerosol optical thickness in Jokioinen and Sodankylä is only 0.08 at 500 nm and rarely exceeds 0.2 indicating a rather clean atmosphere. Therefore, no correction for absorbing aerosols was included in our OMI UV data. Had the currently operational correction for absorbing aerosols been applied, the correction factors for UV irradiance would have been near 0.90 to 0.95 in Jokioinen and 0.99 to 0.97 in Sodankylä for the OMI data in this work.

2.2 Surface UV measurements

The validation of OMI UV algorithm was done with surface UV measurements made in Jokioinen and Sodankylä for years 2005 to 2011. The main reference instruments were Solar Light 501 broadband radiometers, that provided UV index data at one minute fre-

AMTD
8, 487–516, 2015

quency. Additionally, Brewer spectroradiometers co-located with the radiometers were used to calibrate SL501 instruments.

2.2.1 Brewer spectrophotometer

Brewer spectrophotometers MK-III #107 (286.5–365 nm) in Jokioinen and MK-II #037 (290–325 nm) in Sodankylä provided UV index typically once or twice an hour. The Brewer instruments, their calibration and data evaluation procedures are presented in Lakkala et al. (2008). The scrutinous instrument operation and data evaluation yields data accuracy of 5 % compared to the QASUME reference spectroradiometer Lakkala et al. (2008). To obtain UV index from Brewer measurements for the purposes presented in the next section, full irradiance spectra in the erythemal range 290–400 nm are needed. This was done using SHICrivm software package that combines the measured spectra with an adjusted extraterrestial solar spectrum to obtain a standardized irradiance over the erythemal range, similarly as in Tanskanen et al. (2007). The software is available and documented at www.rivm.nl/SHICrivm.

2.2.2 Solar Light 501 radiometer

The surface UV was also measured using Solar Light 501 radiometers, that provide a frequent once per minute, direct observation of UV index. The measurement frequency is crucial here, so that the UV data captures the temporal variability of UV attenuation by clouds near OMI overpass.

The accuracy of a well maintained SL501 is about 7 to 16 % according to Hülsen and Gröbner (2007). These instruments in Jokioinen and Sodankylä are used for monitoring UV index levels and they are maintained with simpler calibration methods and thus our estimate for the accuracy is about 20 %. The most notable error sources include nonideal wavelength response, whose effect depends on ozone column amount and solar zenith angle, and cosine response, that depends on the radiation field itself,

AMTD
8, 487–516, 2015

mostly on the direct to diffuse ratio of UV radiation. Also changes in humidity may affect the response of these instruments.

To achieve a higher data accuracy required for the evaluation of OMI products, an additional SL501 calibration was done near each OMI overpass. For that purpose, the Brewer UV index closest to overpass $\mathrm{UVI}_{\mathrm{Brewer,calib}}$ was matched with three minute averages of SL501 UV index $\mathrm{UVI}_{\mathrm{SL501,calib}}$ to get calibration factor R_{OP}

$$R_{\mathrm{OP}} = \frac{\mathrm{UVI}_{\mathrm{Brewer,calib}}}{\mathrm{UVI}_{\mathrm{SL501,calib}}} \tag{1}$$

The three minute average for $\mathrm{UVI}_{\mathrm{SL501,calib}}$ corresponds to the approximate time in which a Brewer scans the wavelength region from 290–320 nm that contributes most to UVI index via the convolution of the erythemal action function. R_{OP} is assumed to be constant ±30 min near OMI overpass and so, the calibrated SL501 UVI at the overpass is

$$\mathrm{UVI}_{\mathrm{SL501,OP}} = R_{\mathrm{OP}} \cdot \mathrm{UVI}'_{\mathrm{SL501,OP}} \tag{2}$$

where $\mathrm{UVI}'_{\mathrm{SL501,OP}}$ is the ±30 min average of SL501 measurement near Aura overpass and $\mathrm{UVI}_{\mathrm{SL501,OP}}$. is the UV index used to validate OMUVB UV product. The time difference between calibration and overpass was required to be less than 60 min, while it was mostly less than 40 and 15 min on average.

This calibration method was evaluated by comparing the calibrated SL501 3 min UVI to the Brewer UVI observations closest to the calibration (but excluding $\mathrm{UVI}_{\mathrm{Brewer,calib}}$) with ratio

$$R = \frac{\mathrm{UVI}_{\mathrm{Brewer}}}{\mathrm{UVI}_{\mathrm{SL501}}} \tag{3}$$

This is shown in Fig. 1. The leftmost group of boxes in Fig. 1a shows, that when time difference from SL501 calibration is less than 30 min, R is still within ±1 % of R_{OP} for

AMTD
8, 487–516, 2015

clear sky (the leftmost box). Similarly, R is within ±10 % of R_{OP}, excluding outliers, for overcast class (the rightmost box). Thus, it is justified to assume that changes in R_{OP} are small in time for those cases and that we can calibrate SL501 using Brewer UVI within ±30 min from OMI overpass.

Broken sky class (middle boxes) in Fig. 1 a point out that broken sky situation is problematic for the chosen ±30 min time window. This is likely due to the possible rapid changes in UV index during the three minute calibration and Brewer spectral scan, which can result in $UVI_{SL501,calib}$ and R_{OP} which are less representative for the whole ±30 min time window. It is characteristic for broken sky situations, that changes in surface irradiance are large and rapid. When more than 30 min has passed from the calibration in cloudy cases, R_{OP} varies more and this calibration method might not increase SL501 accuracy as desired anymore.

Figure 1b shows a comparison between calibrated SL501 and Brewer UV indices for the same data as in Fig. 1a. The differences are small for overcast (MB = 0.003 UVI, RMSD = 0.10 UVI) and for clear sky situations (MB = −0.01 UVI, RMSD = 0.05 UVI), supporting the conclusion, that R_{OP} can be assumed constant within the time window.

2.3 Measurements for cloudiness classification

In order to examine OMI UV performance in different cloudiness conditions, the data was divided into clear sky (CS), broken sky (BS) and overcast (OC) classes using ground based observations in Jokioinen and Sodankylä at the time of satellite overpass. The method uses sunshine duration SD, cloud cover and standard deviation of global radiation (SD(glob)) to decide the cloudiness from the ground based point of view and an illustration of the classification principle is shown in Fig. 2.

Sunshine duration SD (minutes of bright sunshine per hour) was measured using a Siggelkow Gerätebau SONI sensor. It translates an irradiance of more than 120 $W m^{-2}$ (on a plane perpendicular to direct solar beam) as clear solar disc uncovered by clouds and less than 120 $W m^{-2}$ as cloud covered sun. If SD was between 1

AMTD
8, 487–516, 2015

and 59 min during a time window of ±30 min around Aura satellite overpass, the algorithm decided it was a broken sky situation.

A ±30 min time window was chosen for classification because it produced the statistically best match between satellite and ground based UV index (see Sect. 2.5). Considering cloudiness, a one hour time window allows the prevailing cloud field to drift in the view of a measurement station. For example, in a typical mean wind of 10 ms^{-1} the cloud field travels 36 $km\,h^{-1}$, which roughly corresponds to the dimensions of an OMI pixel. den Outer et al. (2012) used a similar approach when comparing daily UV sums from satellite and ground based point of view. They showed, that for comparison with ground based measurements of daily UV, spaceborn UV product ought to be averaged in an optimal area of about 1 to 1.5°, which corresponds to the temporal UV variations observed at measurement station during 5 to 7 h.

It is to be noted, that sunshine duration alone is not capable of describing cloudiness in the whole upper hemisphere and so, supporting observations were needed for a reliable classification in the cases of clear sky (SD = 60 min) and overcast sky (SD = 0 min).

In those cases the classification took use of synoptic cloud cover observations done either manually every 3 h or automatically twice an hour using a ceilometer that detects clouds up to 7.5 km altitude. Here the classification allows the closest observation to overpass to have 0 to 1 octas cloudiness for clear sky and 7 to 8 octas for overcast, and other cases are determined as broken sky situations. Cloud cover information has its limits, too, since high cirrus cloud may remain undetected by ceilometer and on the other hand, manual cloudiness may reach time differences up to 1.5 h to satellite overpass, during which cloudiness can change.

To tackle these problems we used the variation of global radiation (one minute time resolution) as an indicator of UV attenuation caused by clouds. Here, global radiation means the hemispherical solar irradiance incident on a horizontal surface and the measuring instrument was a Kipp & Zonen pyranometer. A ±30 min standard deviation of 100 $W\,m^{-2}$ was chosen empirically as the upper limit for variation in global radiation in

AMTD
8, 487–516, 2015

clear and overcast conditions to identify broken sky cases, where deviation was typically larger. This is specifically important in situations when high thin cirrus clouds don not reduce the radiation observed by SD sensor under 120 $W m^{-2}$ and are located above the reach of the ceilometer, in which case the algorithm could falsely indentify a cloudy case as clear sky. For an overpass to be accepted to the data set, each three simultaneous classification variables had to exist and they needed to pass a manual check for data consistency.

Figure 3 shows an example day of all ground based observations along with OMI UV index in Jokioinen on the 27 May 2008. Sunshine duration and global radiation show the characteristic rapid variations during broken sky conditions and less variation for clear sky and ovecast situations. Suspicious sunshine duration observation SD = 0 s min^{-1} can be seen between hours 6 and 7, when SD sensor recorded the sun became obscured, while pyranometer (Fig. 3c, blue line) and SL501 (Fig. 3d, red line) recorded no sudden changes in solar irradiance.

When OMI and ground based data sets were combined using the sampling explained above, it yielded 1 to 4 satellite overpasses per day for the evaluation of OMI UV product. In Jokioinen there were 1526 satellite overpasses in total with solar zenith angle ranging from 37 to 70° and 1965 overpasses in Sodankylä, with solar zenith angle between 43 and 75°.

2.4 MODIS cloud data

The difference in the field of view (FOV) between a satellite and a ground based instrument needs to be considered when validating UV cloud attenuation in OMI products, because the satellite instrument might see significantly more clouds or clear areas within its footprint than the ground station in its own FOV.

We consider the ±30 min time window for ground based observations to correspond the instantaneous spatial averages of an OMI footprint, but in addition a satellite based view over the clouds was desired. For that purpose we used additional MODIS cloud cover data (Platnick et al., 2003) from the Aqua satellite in order to independently

AMTD
8, 487–516, 2015

examine the cloudiness from a satellite FOV as if it had been seen by OMI onboard Aura satellite. We think the caveat of these MODIS and OMI being operated on different platforms is tolerable, since Aura and Aqua fly in the same A-train constellation with Aqua only about 15 min before Aura.

We used MODIS Collection 5.1 cloud fraction data, that has a geographical resolution of 5 km × 5 km, to investigate how the cloudiness seen from space compares with our ground-based cloudiness classification. The high resolution of these cloud products allowed detection of possible broken cloudiness within the larger OMI footprint (13 km × 24 km at best). The MODIS cloud fraction data was used to confirm, that when ground based measurements see overcast cloudiness, the OMI would also see a fully cloudy pixel and similarly for clear sky situations, see the Sect. 3.1.

2.5 UV-comparison

The statistical measures for the UV comparison were mean bias MB, relative mean bias rMB

$$\mathrm{rMB} = \frac{\mathrm{MB}}{\overline{\mathrm{UVI}_{\mathrm{SL501,OP}}}} = \frac{\frac{1}{n}\sum_{i=1}^{n}\left(\mathrm{UVI}_{\mathrm{OMI}}(i) - \mathrm{UVI}_{\mathrm{SL501,OP}}(i)\right)}{\overline{\mathrm{UVI}_{\mathrm{SL501,OP}}}} \quad (4)$$

relative error

$$\mathrm{rE} = \frac{1}{n}\sum_{i=1}^{n}\left[\frac{\mathrm{UVI}_{\mathrm{OMI}}(i) - \mathrm{UVI}_{\mathrm{SL501,OP}}(i)}{\mathrm{UVI}_{\mathrm{SL501,OP}}(i)}\right] \quad (5)$$

root mean square difference RMSD, relative RMSD

$$\mathrm{rRMSD} = \frac{\mathrm{RMSD}}{\overline{\mathrm{UVI}_{\mathrm{SL501,OP}}}} = \frac{\sqrt{\frac{1}{n}\sum_{i=1}^{n}\left(\mathrm{UVI}_{\mathrm{OMI}}(i) - \mathrm{UVI}_{\mathrm{SL501,OP}}(i)\right)^2}}{\overline{\mathrm{UVI}_{\mathrm{SL501,OP}}}} \quad (6)$$

AMTD
8, 487–516, 2015

correlation coefficient and average standard deviation of UVI difference SD(diff) during one hour.

As mentioned, $UVI_{SL501,OP}$ was averaged for ±30 min near overpass. This is because that time window gave optimal statistic discrepancies between OMI UV index and SL501 UV index, as illustrated in Fig. 4. Figure 4a shows, that the average the bias (MB and rMB) and variability (RMSD and rRMSD) of OMI UVI vs. SL501 UVI are close to their minima near 60 min averaging time window (±30 min near satellite overpass). Further, a high correlation and low standard deviation of UVI difference SD(diff) in Fig. 4b at 60 min time window also support that conclusion. Therefore, ±30 min time averaging was considered optimal for ground based UV data, which is then also a logical choice for considering sunshine duration and global radiation data in cloudiness classification. Kazadzis et al. (2009a) also concluded, that a longer averaging time window can improve the statistics of an OMI to ground based UV comparison, when they looked at the variability of surface irradiance measurements in an area similar to an OMI footprint.

3 Results

3.1 Cloudiness classification results

Using the cloudiness algorithm presented in Sect. 2.3 the satellite overpasses in Jokioinen (Sodankylä) were divided into the three cloudiness classes as follows: 8.9 % (4.7 %) to clear sky, 73.2 % (64.7 %) to broken sky and 17.9 % (30.5 %) to overcast class (see Table 1). This classification was manually inspected and corrected for misinterpretations in 167 cases out of 3491 overpasses (4.7 %) mainly for cirrus situations, that were falsely decided as clear situations. For the most interesting overcast class we have in total 873 overpasses from 488 summer days.

The cloudiness classification method presented in Sect. 2.3 can detect small clouds and small clear areas that the classification based only on sunshine duration can not

AMTD
8, 487–516, 2015

see in clear sky and overcast situations, correspondingly. As a result, our algorithm revealed, that 48 % of the SD = 60 min (clear sky according to only SD) and 7 % of the SD = 0 min (overcast according to only SD) observations were in fact broken sky cases. This shows, that sunshine duration alone can make a singificant number of false clear sky interpretations when cloud cover is small and under thin cirrus cloud conditions.

There is, unfortunately, no accurate and comprehensive way to validate the classification method. However, as sunshine duration, synoptic cloudiness and global radiation together describe the cloud attenuated signal from the whole sky and with a high frequency, the method can be assumed to produce a good estimate of cloudiness from the ground based point of view.

We used a temporal average in the time window of ±30 min for ground based observations to represent the large instantaneous field of view of the satellite instrument. Related to this, Krotkov et al. (2001) pointed out a statistical error source, which occurs due to the different fields of view of a satellite and surface instruments. Namely, when the ground instrument sees 0 % cloud cover, the satellite may see more than 0 % with its larger FOV, but obviously not less than that. This is illustrated in Fig. 5, where clouds not seen by ground based instruments result in lower satellite estimates for surface UV. Likewise, when the ground instrument sees 100 % cloud cover, the satellite may see less than that, but not more.

This bias was observed in clear sky cases, when OMI CMF was less than one in numerous situations. However, there were only few overpasses (with CMF between 0.80 and 0.93) when OMI UVI was notably lower than SL501 UVI in CMF = 1 cases and these overpasses were removed form the analysis. Another thirteen clear sky overpasses were rejected, when the MODIS cloud fraction product revealed clouds in an area representing an OMI footprint, but it had no significant effect on the statistics in the UV comparison. In other words, while the FOV related statistical CMF bias was observed in clear sky cases, it appeared to have little effect on these results when comparing UVI from OMI and SL501.

AMTD
8, 487–516, 2015

As explained, the similar CMF bias is expected also in overcast class, but its indentification is more difficult, as the true CMF is unknown for full cloud cover. To identify possible clear sky areas located inside the OMI footprint, but not seen by ground based instruments, we used fine resolution MODIS Aqua cloud data from an area corresponding an OMI footprint. MODIS revealed a cloud fraction of less than 100 % in only ten overcast OMI overpasses and, after these cases were removed from the analysis, we believe that the remaining overcast OMI UV index data is not significantly affected by clear sky patches within the FOV.

One might argue, that allowing cloud cover of 1/8 for clear sky and 7/8 for overcast in cloudiness classification algorithm (Fig. 2) would increase this statistical bias. Excluding these cases from clear sky and overcast cases, however, did not effect the OMI UVI to SL501 UVI differences significantly. This may result from the fact that even the smallest observable patches of cloud or cloud free sky will result in cloud cover observation of 1/8 and 7/8, respectively. Also, the patches did not appear in front of the sun (SD = 60 and SD = 0).

3.2 UV comparison results

The main results for OMI UV validation using SL501 are presented in Figs. 6 and 7 and in Table 1. For both Jokioinen and Sodankylä OMI UV overestimates the surface UV index systematically compared to measurements by MB = 0.44 UVI and MB = 0.22 UVI, respectively.

While the absolute bias in clear sky cases is similar to that of overcast cases, the difference is larger in relative sense (eg. rMB for clear skies is 0.12 and 0.39 for overcast in Jokioinen) due to lower average UVI in overcast situations. This indicates, OMI estimates for UV index too high compared to SL501 and that is related to cloudiness in overcast situations. The sampling based on ground instruments and supported by MODIS cloud product is to ensure that both OMI and ground instruments have entirely cloud covered views. Thus, the UVI bias in overcast conditions is also not explained

AMTD
8, 487–516, 2015

by the satellite instrument OMI seeing clear sky patches that remain undetected in the ground based FOV.

The positive OMI UV bias seen in clear sky cases has been studied by eg. Cachorro et al. (2010) and Kazadzis et al. (2009a). Part of it may be due to aerosol absorption not accounted for by OMI, but that is not likely enough to explain the whole bias in Sodankylä and Jokioinen since aerosol loadings there are typically small (Aaltonen et al., 2012). Whatever the reason behind clear sky bias is, it is not enough to explain the positive bias seen in the main focus of this study, the overcast situations. Also, Arola et al. (2009) presented the climatological correction for UV absorption by aerosols, that is now applied for the currently available OMI UV products. The correction factors for absorbing aerosols in the summer months in Jokioinen and Sodankylä are about 0.90 and 0.97, correspondingly, which is less than the positive bias in OMI UV index (see relative error rE in Table 1). It is not enough to explain the cloud related OMI bias.

Largest random errors (RMSD, Table 1) occur in broken sky cases as you may expect, remembering the large variability of UV index in those cases. The variability can make the ±30 min time average of the ground based UVI less representative of the instantaneous OMI footprint UVI and also adds uncertainty to our SL501 calibration method. However, the largest random errors in relative sense (rRMSD) are found in overcast situations. This, again, is not explained by FOV related cloud cover bias as discussed in Sect. 3.1.

As discussed in Sect. 3.1, the cloudiness classification method presented in this paper detected broken sky conditions that would have been falsely interpreted as clear sky or overcast by sunshine duration observations alone. In some of these special cases OMI underestimated UV index notably, since clouds were present within OMI footprint, but the clouds did not obscure the sun as seen from SL501. If these broken sky cases were not detected and removed, OMI UVI performance in clear sky conditions would show smaller UVI bias (MB = 0.19 UVI compared to MB = 0.26 UVI in Sodankylä) and more scatter (SD(diff) = 0.22 UVI compared to SD(diff) = 0.13 UVI in Sodankylä) similarly to broken sky situations.

AMTD
8, 487–516, 2015

While the current OMI algorithm calculates the cloud modification factor CMF by assuming plane parallel water clouds (see Sect. 2.1), earlier versions of satellite based UV products assumed a CMF for lambertian clouds with an equivalent reflectivity LER. Cloud modification factor based on LER assumption is defined as

$$\mathrm{CMF}_{\mathrm{LER}} = \frac{1 - R_{360}}{1 - R_{\mathrm{surf}}} \tag{7}$$

where R_{360} is the earth reflectivity observed from satellite and R_{surf} is the surface albedo from the albedo climatology. Thus, $\mathrm{CMF}_{\mathrm{LER}}$ does not consider the wavelength dependence of CMF arising from ozone absorption and molecular scattering, while the PPA CMF does. The comparison of OMI UVI with SL501 UVI between PPA and LER cloud assumptions is shown in Fig. 8a and b, respectively. Figure 8 shows that while there is little difference in UVI ratio in clear sky cases, overcast cases show notably smaller UVI bias for LER (MB = 0.043 UVI) estimate than for PPA (MB = 0.45 UVI). Krotkov et al. (2001) noted similarly, that the PPA cloud model overestimates CMF a bit more than LER model for small CMF values when the TOMS satellite UV algorithm was compared to ground based estimates for CMF. This is in line with our finding from Fig. 8.

In addition to UV index observed with SL501 radiometers, Brewer UVI index was available near Aura satellite overpass time. Statistical measures showed, that in cloud free situation OMI UVI compared equally well with SL501 and Brewer UVI. However, in cloudy cases OMI UVI random errors are greater when compared with Brewer than with SL501, while bias was still relatively unchanged. We believe this was due to SL501 having a more frequent UVI sampling near satellite overpass than Brewer, thus a one hour average for SL501 captures better possible variations in the cloud layers and represents better a spatial average seen from by OMI.

AMTD
8, 487–516, 2015

4 Conclusions

The OMI UV product was validated using Solar Light 501 surface UV index measurements at the time of satellite overpass at Jokioinen and Sodankylä. The data set covers the summers 2005–2011 with nearly 3500 overpasses at the two ground stations in total. The goal was to further investigate the existence and reasons of the cloud related positive UV bias found in previous studies in more detail.

In line with previous studies we found that OMI UV product generally overestimates the surface UV index by rMB = 0.15 UVI in Jokioinen and rMB = 0.11 UVI in Sodankylä, while the correlation is still rather good (0.94 and 0.95).

We used additional ground based measurements of sunshine duration, cloud cover and global radiation to deduce cloudiness during overpass (clear sky, broken sky and overpass) to study the effects of cloudiness on OMI UV performance. Using all three observations to classify cloudiness was more accurate in revealing broken sky conditions when sunshine duration alone suggested a clear sky or an overcast situation. However, in terms of OMI UV index performance compared to SL501 radiometer this better separated cloudiness classes show quite similar results as when cloudiness is classified with the more simple approach.

There is a slightly smaller overestimation in clear sky cases and a significantly larger relative overestimation under overcast skies (rMB = 0.39 for Jokioinen and rMB = 0.29 for Sodankylä), which indicates a cloud related positive bias in OMI UV index. Technically, CMF seems to be biased high. We concluded that the cloud related positive UVI bias is not in this case fully explained by aerosol absorption, or by the positive CMF bias due to clear areas in cloud cover observed only by OMI, but not by the ground based instruments. The latter was determined using co-located, MODIS cloud fraction data from Aqua satellite. Because similar performance for OMI UVI was seen also with a more simple SD based classification, it indicates, that increased overestimation by OMI during overcast cases is due to the presence of clouds and is not mainly due clear sky patches within the OMI pixel.

AMTD
8, 487–516, 2015

One likely source of error is, that OMI UV algorithm assumes a homogeneous plane parallel cloud layer, which may, however, be unusual in the real atmosphere. Genkova and Davies (2003) used cloud reflectance data from MISR instrument to show, that midmorning clouds have a spatially reasonably uniform reflectance in only about 1/70 of cases in a conventional footprint of a satellite instrument. Thus, deviations from a plane parallel cloud are common enough to be a significant error source in a large data set.

The mechanism of cloud related positive OMI UVI bias was not entirely solved in this study, but it is now clear that the bias exists and is enhanced in well defined overcast cases. Further investigation of the issue could be set up by trying to separate the bias into components related to the inversion of cloud optical thickness, and into the forward calculation of the cloud modification factor and surface UV.

Acknowledgements. The authors thank the OMI International Science Team for the satellite data used in this study.

References

Aaltonen, V., Rodriguez, E., Kazadzis, S., Arola, A., Amiridis, V., Lihavainen, H., and de Leeuw, G.: On the variation of aerosol properties over Finland based on the optical columnar measurements, Atmos. Res., 116, 46–55, doi:10.1016/j.atmosres.2011.07.014, 2012. 492, 502

Antón, M., Cachorro, V. E., Vilaplana, J. M., Toledano, C., Krotkov, N. A., Arola, A., Serrano, A., and de la Morena, B.: Comparison of UV irradiances from Aura/Ozone Monitoring Instrument (OMI) with Brewer measurements at El Arenosillo (Spain) – Part 1: Analysis of parameter influence, Atmos. Chem. Phys., 10, 5979–5989, doi:10.5194/acp-10-5979-2010, 2010. 489

Arola, A., Kazadzis, S., Krotkov, N., Bais, A., Gröbner, J., and Herman, J. R.: Assessment of TOMS UV bias due to absorbing aerosols, J. Geophys. Res.-Atmos., 110, D23211, doi:10.1029/2005JD005913, 2005. 492

Arola, A., Kazadzis, S., Lindfors, A., Krotkov, N., Kujanpaa, J., Tamminen, J., Bais, A., di Sarra, A., Villaplana, J. M., Brogniez, C., Siani, A. M., Janouch, M., Weihs, P., Webb, A.,

AMTD
8, 487–516, 2015

Koskela, T., Kouremeti, N., Meloni, D., Buchard, V., Auriol, F., Ialongo, I., Staneck, M., Simic, S., Smedley, A., and Kinne, S.: A new approach to correct for absorbing aerosols in OMI UV, Geophys. Res. Lett., 36, L22805, doi:10.1029/2009GL041137, 2009. 492, 502

Buchard, V., Brogniez, C., Auriol, F., Bonnel, B., Lenoble, J., Tanskanen, A., Bojkov, B., and Veefkind, P.: Comparison of OMI ozone and UV irradiance data with ground-based measurements at two French sites, Atmos. Chem. Phys., 8, 4517–4528, doi:10.5194/acp-8-4517-2008, 2008. 489

Cachorro, V. E., Toledano, C., Antón, M., Berjón, A., de Frutos, A., Vilaplana, J. M., Arola, A., and Krotkov, N. A.: Comparison of UV irradiances from Aura/Ozone Monitoring Instrument (OMI) with Brewer measurements at El Arenosillo (Spain) – Part 2: Analysis of site aerosol influence, Atmos. Chem. Phys., 10, 11867–11880, doi:10.5194/acp-10-11867-2010, 2010. 489, 492, 502

den Outer, P. N., van Dijk, A., Slaper, H., Lindfors, A. V., De Backer, H., Bais, A. F., Feister, U., Koskela, T., and Josefsson, W.: Applying spaceborne reflectivity measurements for calculation of the solar ultraviolet radiation at ground level, Atmos. Meas. Tech., 5, 3041–3054, doi:10.5194/amt-5-3041-2012, 2012. 496

Genkova, I. and Davies, R.: Spatial heterogeneity of reflected radiance from globally distributed clouds, Geophys. Res. Lett., 30, 2096, doi:10.1029/2003GL018194, 2003. 505

Hülsen, G. and Gröbner, J.: Characterization and calibration of ultraviolet broadband radiometers measuring erythemally weighted irradiance, Appl. Optics, 46, 5877–5886, doi:10.1364/AO.46.005877, 2007. 493

Ialongo, I., Casale, G. R., and Siani, A. M.: Comparison of total ozone and erythemal UV data from OMI with ground-based measurements at Rome station, Atmos. Chem. Phys., 8, 3283–3289, doi:10.5194/acp-8-3283-2008, 2008. 489

Ialongo, I., Arola, A., Kujanpää, J., and Tamminen, J.: Use of satellite erythemal UV products in analysing the global UV changes, Atmos. Chem. Phys., 11, 9649–9658, doi:10.5194/acp-11-9649-2011, 2011. 488, 489

Kazadzis, S., Bais, A., Arola, A., Krotkov, N., Kouremeti, N., and Meleti, C.: Ozone Monitoring Instrument spectral UV irradiance products: comparison with ground based measurements at an urban environment, Atmos. Chem. Phys., 9, 585–594, doi:10.5194/acp-9-585-2009, 2009a. 489, 499, 502

Kazadzis, S., Bais, A., Balis, D., Kouremeti, N., Zempila, M., Arola, A., Giannakaki, E., Amiridis, V., and Kazantzidis, A.: Spatial and temporal UV irradiance and aerosol vari-

AMTD
8, 487–516, 2015

ability within the area of an OMI satellite pixel, Atmos. Chem. Phys., 9, 4593–4601, doi:10.5194/acp-9-4593-2009, 2009b. 489

Krotkov, N. A., Herman, J. R., Bhartia, P. K., Fioletov, V., and Ahmad, Z.: Satellite estimation of spectral surface UV irradiance 2. Effects of homogeneous clouds and snow, J. Geophys. Res., 106, 11743–11759, doi:10.1029/2000JD900721, 2001. 491, 492, 500, 503

Lakkala, K., Arola, A., Heikkilä, A., Kaurola, J., Koskela, T., Kyrö, E., Lindfors, A., Meinander, O., Tanskanen, A., Gröbner, J., and Hülsen, G.: Quality assurance of the Brewer spectral UV measurements in Finland, Atmos. Chem. Phys., 8, 3369–3383, doi:10.5194/acp-8-3369-2008, 2008. 493

Lindfors, A. and Arola, A.: On the wavelength-dependent attenuation of UV radiation by clouds, Geophys. Res. Lett., 35, L05806, doi:10.1029/2007GL032571, 2008. 492

Platnick, S., King, M., Ackerman, S., Menzel, W., Baum, B., Riedi, J., and Frey, R.: The MODIS cloud products: algorithms and examples from Terra, IEEE T. Geosci. Remote, 41, 459–473, doi:10.1109/TGRS.2002.808301, 2003. 497

Stammes, P. and Noordhoek, R.: OMI Algorithm Theoretical Basis Document. Clouds, Aerosols, and Surface UV Irradiance, Volume III, available at: http://eospso.gsfc.nasa.gov/sites/default/files/atbd/ATBD-OMI-03.pdf (last access: 12 January 2015), 2002. 491

Tanskanen, A., Krotkov, N., Herman, J., and Arola, A.: Surface ultraviolet irradiance from OMI, IEEE T. Geosci. Remote, 44, 1267–1271, doi:10.1109/TGRS.2005.862203, 2006. 488, 491, 492

Tanskanen, A., Lindfors, A., Maatta, A., Krotkov, N., Herman, J., Kaurola, J., Koskela, T., Lakkala, K., Fioletov, V., Bernhard, G., McKenzie, R., Kondo, Y., O'Neill, M., Slaper, H., den Outer, P., Bais, A. F., and Tamminen, J.: Validation of daily erythemal doses from Ozone Monitoring Instrument with ground-based UV measurement data, J. Geophys. Res.-Atmos., 112, D24S44, doi:10.1029/2007JD008830, 2007. 493

Weihs, P., Blumthaler, M., Rieder, H. E., Kreuter, A., Simic, S., Laube, W., Schmalwieser, A. W., Wagner, J. E., and Tanskanen, A.: Measurements of UV irradiance within the area of one satellite pixel, Atmos. Chem. Phys., 8, 5615–5626, doi:10.5194/acp-8-5615-2008, 2008. 489

AMTD
8, 487–516, 2015

Table 1. Statistics from UV index comparison between OMI and the reference SL501 ($UVI_{SL501,OP}$, see Eq. 2) for the entire data set used. See Sect. 2.5 for the statistical definitions.

Jokioinen	clear	broken	overcast	all
Number	136	1117	273	1526
% of total	8.9	73.2	17.9	100.0
MB	0.50	0.44	0.45	0.44
rMB	0.12	0.14	0.39	0.15
RMSD	0.53	0.69	0.64	0.67
rRMSD	0.12	0.22	0.54	0.23
rE %	12.1	18.1	56.0	24.3
corr	0.99	0.90	0.78	0.94
SD(diff)	0.17	0.54	0.45	0.50
Sodankylä				
Number	93	1272	600	1965
% of total	4.7	64.7	30.5	100.0
MB	0.26	0.19	0.28	0.22
rMB	0.09	0.08	0.29	0.11
RMSD	0.29	0.44	0.42	0.43
rRMSD	0.10	0.18	0.44	0.22
rE %	8.6	10.5	39.0	19.1
corr	1.00	0.92	0.87	0.95
SD(diff)	0.13	0.40	0.32	0.37

AMTD
8, 487–516, 2015

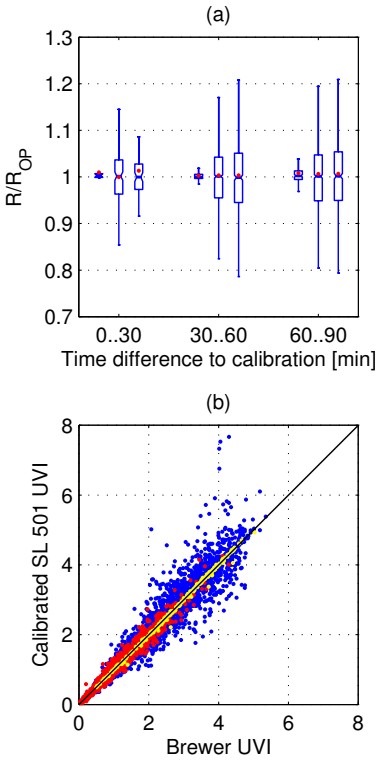

Figure 1. (a) Relative calibration coefficients R/R_{OP} in Sodankylä as a function of the time difference between SL501 calibration and a nearby Brewer measurement. Leftmost boxes of each group correspond to clear sky, middle boxes to broken sky and rightmost boxes to overcast classes. The bottom, center and top of each box shows 25th, 50th and 75th percentiles, correspondingly, and the whisker length is 1.5 × interquartile range and red dots show mean values. **(b)** Calibrated SL501 UV index vs. nearby Brewer UVI for data points in **(a)**, yellow represents clear sky, red overcast and blue broken sky situations.

AMTD
8, 487–516, 2015

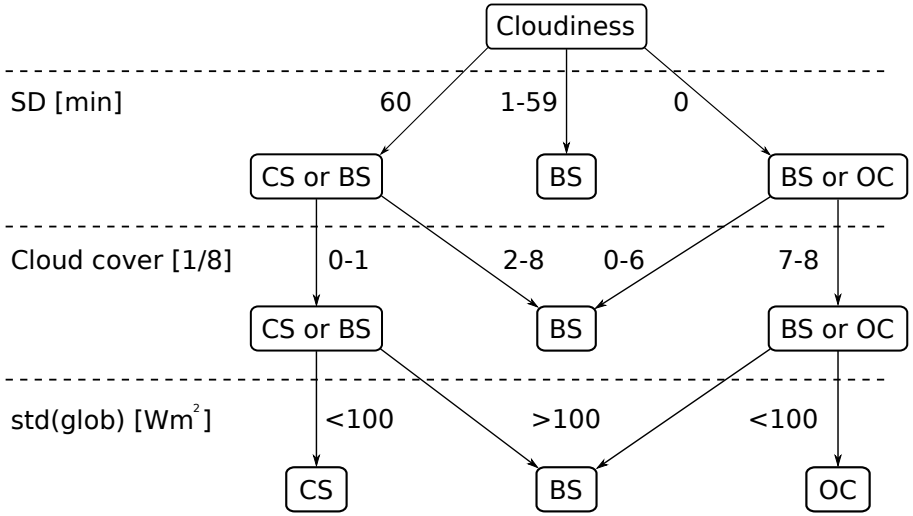

Figure 2. Cloudiness classification using sunshine duration SD, synoptic cloud cover observations and standard deviation of global radiation SD(glob). Cloudiness is deduced to clear sky (CS), broken sky (BS) and overcast (OC) according to threshold values of the observations.

AMTD
8, 487–516, 2015

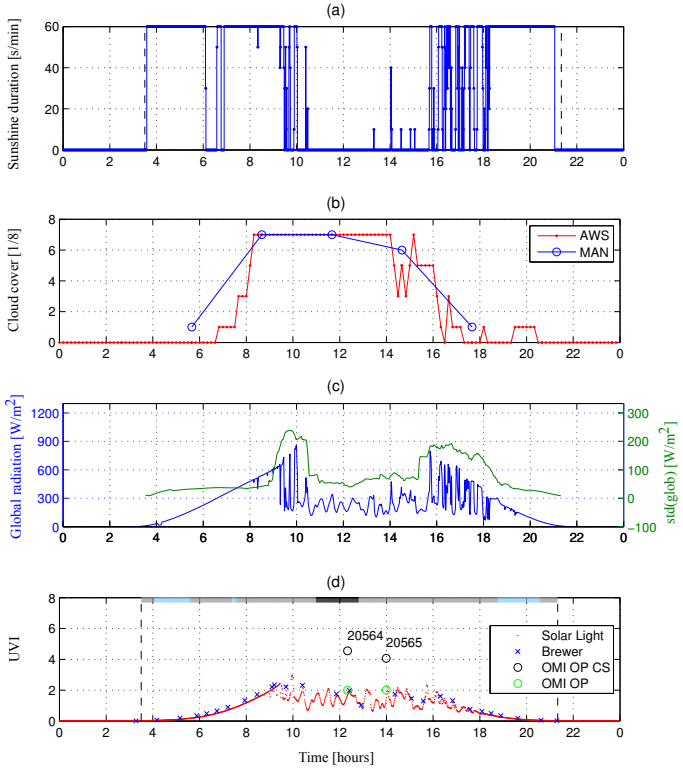

Figure 3. An example overview of ground based observations and OMI UV product on the 27 May 2008 in Jokioinen. **(a)** Sunshine duration, **(b)** visual MAN and ceilometer AWS synoptic cloudiness observation, **(c)** global radiation and ±30 min standard deviation of global radiation and **(d)** UV index from SL501, Brewer, OMI clear sky (OMI OP CS along with orbit number) and OMI cloud corrected (OMI OP). Horizontal bar on the top of **(d)** identifies the cloud classification result for clear sky (blue), broken sky (grey) and overcast (black). Dashed vertical lines indicate sunrise and sunset.

AMTD
8, 487–516, 2015

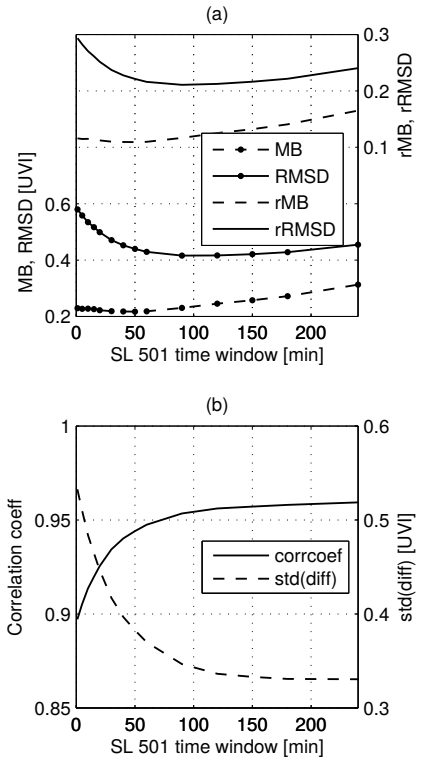

Figure 4. (a) MB, rMB, RMSD and rRMSD and **(b)** correlation coefficient and standard deviation between SL and OMI as functions of the length of the SL501 averaging time window. The data is for all sky cases in Sodankylä during summers 2005–2011.

AMTD
8, 487–516, 2015

OMI UV index in cloudy and cloud-free conditions

M. R. A. Pitkänen et al.

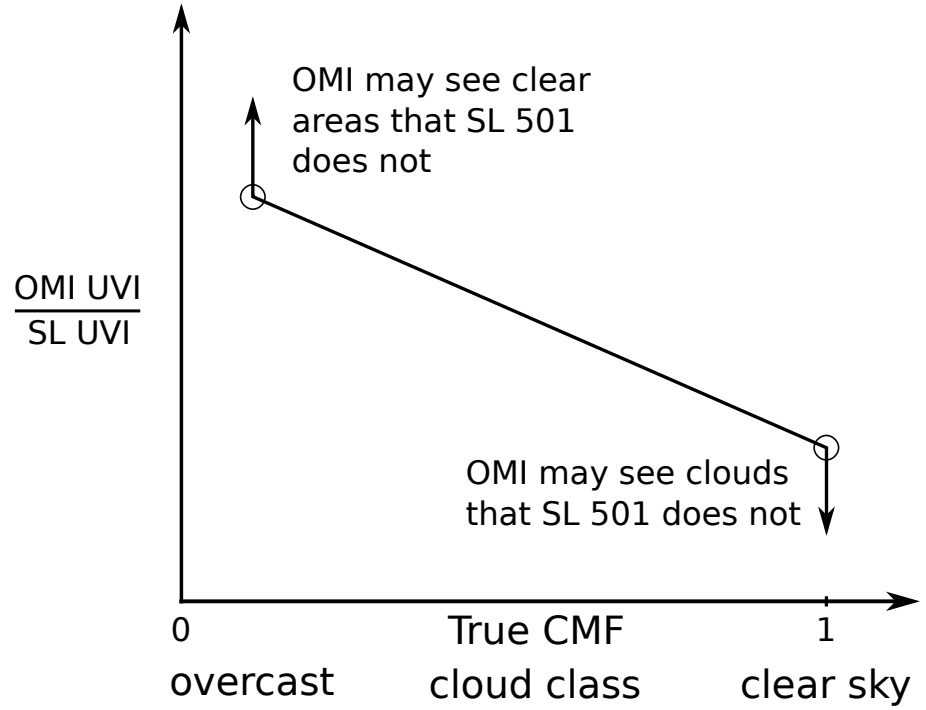

Figure 5. Principle of the UVI index bias due to different field of view of a satellite and ground based instrument.

AMTD
8, 487–516, 2015

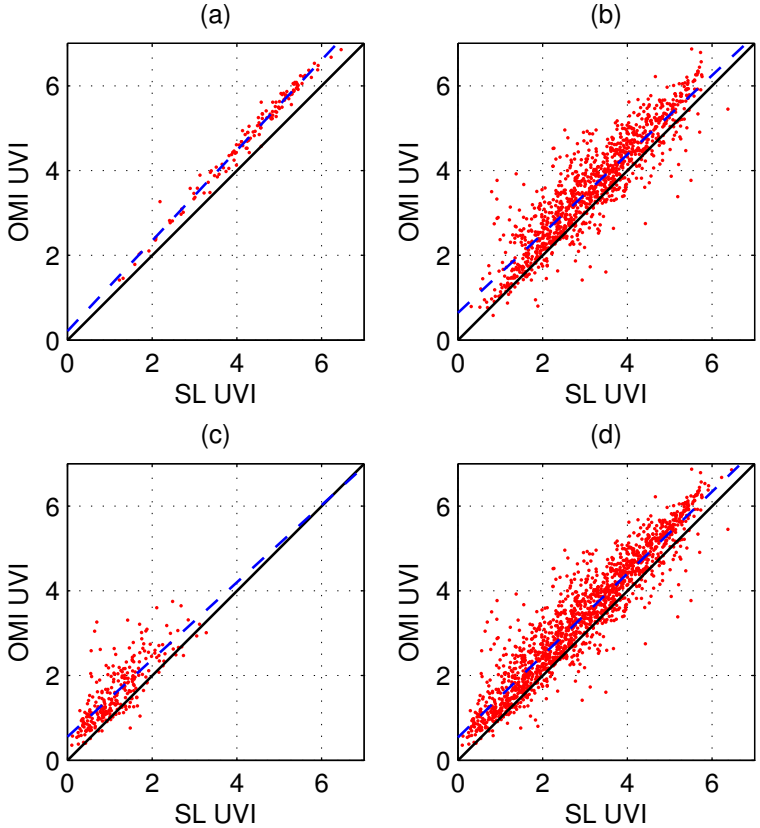

Figure 6. SL-OMI UV index comparison in Jokioinen for **(a)** clear sky, **(b)** broken sky, **(c)** overcast and **(d)** all sky situations. Blue dashed lines represent linear fits to the data.

AMTD
8, 487–516, 2015

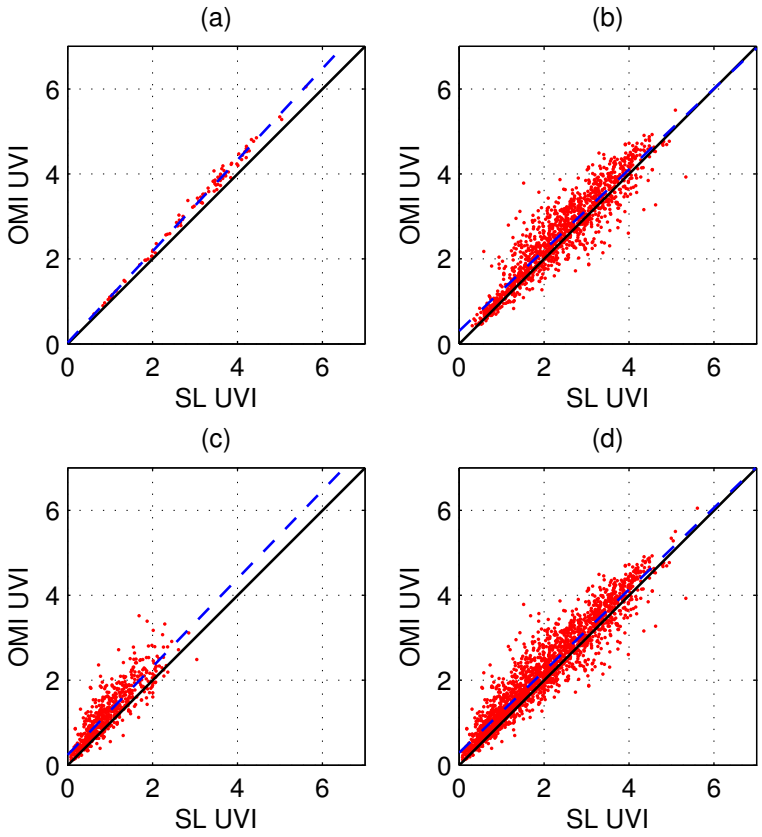

Figure 7. SL-OMI UV index comparison in Sodankylä for **(a)** clear sky, **(b)** broken sky, **(c)** overcast and **(d)** all sky situations. Blue dashed lines represent linear fits to the data.

AMTD
8, 487–516, 2015

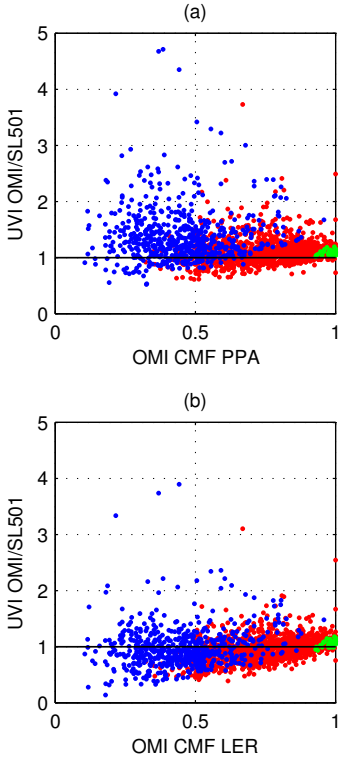

Figure 8. OMI UV index to SL501 UV index ratio comparison when cloud attenuation in OMI product was calculated using **(a)** PPA and **(b)** LER cloud modification factor in Sodankylä. *x* axis shows the corresponding OMI CMF and colored dots present the different cloudiness classes: clear sky (green), broken sky (red) and overcast (blue).

AMTD
8, 487–516, 2015

OMI UV index in cloudy and cloud-free conditions

M. R. A. Pitkänen et al.